Advanced robust control techniques for the stabilization of translational oscillator with rotational actuator based barge-type OFWT

Syed Awais Ali Shah[1], Bingtuan Gao[1] , Nigar Ahmed[2] and Chuande Liu[1]

Abstract
In recent times, renewable energy demand is rapidly increasing worldwide. Offshore wind energy is one of the alternative solutions to the problems posed by non-renewable energy resources. The kinetic energy of the wind is converted to mechanical energy by using an offshore floating wind turbine (OFWT). The efficiency of the OFWT is dependent upon the vibrational effect induced by the environment. In this paper, for the mitigation of this vibrational effect, a new model of barge-type OFWT is designed by using an active control strategy called translational oscillator with a rotational actuator (TORA). The disturbance observer (DO) based advanced control techniques including robust backstepping sliding mode control (BSMC), backstepping integral sliding mode control (BISMC), backstepping nonsingular terminal sliding mode control (BNTSMC), and a new backstepping integral nonsingular terminal sliding mode control (BINTSMC) technique, are devised for the stabilization of OFWT model. The comparison of these techniques is carried out by using MATLAB/SIMULINK which validates the feasibility and correctness of the proposed OFWT model and control techniques.

Introduction

The requirement of clean and renewable energy is becoming necessary around the world due to climate change and the growing energy demand. Wind energy seeks the attention of researchers in recent years and has become the most promising renewable energy resource.[1] Typically, the land-based wind turbines are the source of mostly generated wind power, which is generally installed in sparsely populated and vast areas. In many countries, residents live in coastal areas, where offshore wind energy is easily attainable as compare to land.[2] The speed of the offshore wind is normally faster and steadier than on land. Generally, a 15-mph wind turbine generates twice the energy as compared to a 12-mph wind turbine which means, a small increase in wind speed can cause large energy production. Due to the steadier supply of wind, the wind turbines have been gradually shifted to coastal areas. Since the last decade, mostly wind power turbine setup is established in a shallow sea,[3] but it is mostly criticized due to visual, noise pollution, high construction costs, and complex structures.[4] To eradicate these issues, offshore floating wind turbines (OFWT) were installed in the deep-sea area. In the deep-sea area, it is easy to establish a large wind farm by joining tens to hundreds of floating wind turbines for the improvement of power generation efficiency. For the development of the offshore wind energy system, the wind turbine structure has paramount importance. Nearshore fixed-bottom and deep-sea offshore floating wind turbines are the two broad categories of wind turbines being used.[5] The suction bucket, gravity-based structure, and monopile are the well-known fixed-bottom nearshore wind turbines.[4] In the shallow sea application, these structures are considered suitable but due to their higher cost,

[1]School of Electrical Engineering, Southeast University, Nanjing, P.R. China
[2]College of Automation Engineering, Nanjing University of Aeronautics and Astronautics, Nanjing, P.R. China

Corresponding author:
Bingtuan Gao, School of Electrical Engineering, Southeast University, No. 2 Sipailou, Nanjing 210096, P.R. China.
Email: gaobingtuan@seu.edu.cn

they are not desirable for more than approximately 60 m. Therefore, for deep-sea applications, barge type platform, tension-leg platform, and spar platforms are floating wind turbines that use mooring lines as the supporting structure and can be installed up to 900 m into the deeper water.[6] Nonetheless, offshore floating wind turbine structures are still at an initial development stage and they are being tested with a scale model in the laboratory or real condition with a proof-of-concept study.

The harsh marine environment induces an extreme load onto the offshore floating wind turbines and causes the vibration effect.[7] It is challenging for designers to mitigate the vibration effect from the turbine, which is responsible for large tilt motion that results in the huge load at the tower bottom and blade roots. Thus, to reduce or mitigate the vibration effect from such types of structures, some control techniques have been developed for the last few decades.[8,9] In general, there are three main strategies of control structures that are usually adopted to design the control technique including passive control, semi-active control, and active control.[8] Control structure that uses constant parameters and no energy input is called passive structural control. The basic example of passive structure control is a tuned mass damper (TMD), where its working principle is to absorb the energy from the entire natural frequency of the structure.[10] To achieve better performance and more flexibility than the passive structure control, the authors have applied a semi-active control approach for minimizing structure vibration.[11] The semi-active control approach uses the feedback through sensor output, which measures the structure response and tunes the parameters of the device with a proper control algorithm. Among the three control techniques, the active structure control is more efficient.[9,12] The active control can be categorized into hybrid mass damper (HMD) and active mass damper (AMD). In a hybrid mass damper control method, a controlled force actuator is attached to TMD for achieving better results.[10] The combination of mass and actuator in such a way that the actuator provides both damping and restoring forces on the mass is called an active mass damper, where the control algorithm is designed to control the actuator force.[13]

Murtagh et al.[14] used the tuned mass damper technique for the vibration control of wind turbines. Where the authors have concluded that by tuning the tuned mass damper properly with the predominant frequency, the reduction in the vibration can be achieved. The author, Stewart[15] has worked on four offshore wind turbines by using TMD for reducing environmental loads. Moreover, the author has provided a detailed analysis of the OFWT dynamics. Most of the previous literature for the stabilization of the offshore wind turbine is based on passive control techniques.[16,17] The authors Huang et al.[18] and Arrigan et al.[19] used the

retuned semi-active TMDs in real-time using the short-time Fourier Transform control technique for reducing the vibrations of wind turbine blades. To reduce the vibrational effect from the nacelle/tower of the spar type floating wind turbine, Dinh et al.[20] studied the effect of single and multiple semi-active TMDs. In other studies, the authors have carried out the comparison of TMD and semi-active TMD for the effective oscillation attenuation from offshore wind turbines.[21,22] Lackner et al.[6] briefly explain possible structure control techniques. Additionally, the authors have discussed the effect of barge-type offshore floating wind turbines by using a hybrid mass damper into the nacelle. Si and Karimi[23] has designed a gain scheduling H_2/H_∞ state feedback controller for HMD and installed it at the top of the spar-type floating wind turbine for load mitigation purpose. The hybrid mass damper technique is analyzed and compared with the passive TMD control technique in several research articles.[24,25] They have investigated that the HMD control approach for the alleviation of the floating wind turbine oscillation is better than the passive TMD.

The mechanical systems having less control input than the number of configuration variables are called underactuated mechanical systems. Such types of systems are very appealing due to their cost-efficiency since there are fewer actuators to be dealt with. However, the control design for the underactuated systems is a challenging task as compared to fully actuated systems. The underactuated system has become an attractive research area for the last three decades due to energy saving, increasing the system flexibility, and reducing the cost factor.[26] In this article, the OFWT is modeled by Translational Oscillator with Rotating Actuator (TORA) which is an underactuated nonlinear system. Here the idea is: considering the body of OFWT as the translational cart and adding a rotor into the nacelle yield a kind of TORA. The TORA is an active mass damper (AMD) control scheme, which consists of an unactuated transnational cart and an actuated eccentric rotational proof mass, as shown in Figure 1. In TORA, the angular position of the rotor is controlled by using torque as controlled input. This will eventually result in the stabilization of the translational position of the cart. Initially, the TORA was planned to simplify the dual-spin spacecraft model[27] for capturing the resonance phenomenon and achieving the successful despin maneuver. In Yu et al.,[28] the authors have studied TORA as an AMD, for vibration control of the building. There have been several linear and nonlinear control techniques devised for TORA. Since the TORA consists of non-linearities for which the linear control techniques fail. The feedback linearization technique is also used for TORA, but it is not robust against model uncertainties. Consequently, a more sophisticated control algorithm like backstepping is proposed for the stabilization of TORA. Moreover, different researchers have applied
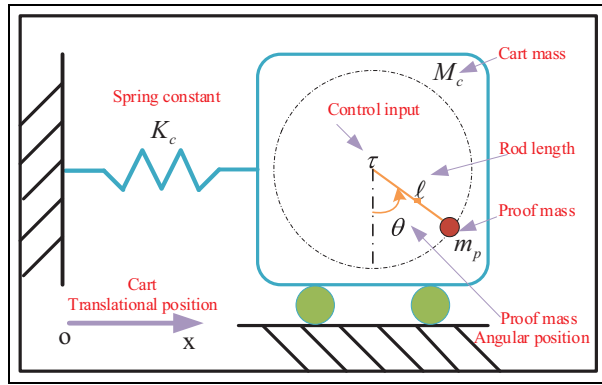
Figure 1. Schematic of TORA.

robust control algorithms like sliding mode control technique, integral sliding mode control, and terminal sliding mode control on TORA.[29–33]

To cancel out or suppress the effect of perturbation or disturbances is an important part of the non-linear control systems. In Yang et al.,[34] Raach et al.,[35] and Zhang et al.,[36] different researchers have used the various non-linear control algorithms like fuzzy control, model predictive control, sliding mode control to prevent the disturbance effect from the OFWT model. As the sliding mode control is robust to matched disturbances and sensitive to mismatched disturbances. So it is difficult to handle mismatched disturbances without applying any disturbance observer. In Shtessel et al.[37] and Li et al.,[38] different methods of estimation and rejection of matched and mismatched disturbances with robust control techniques are described. The main contribution of this research work is, to introduce TORA as an active control approach in the field of the offshore floating wind turbine by considering the body of OFWT as a translational cart and adding a rotor into the nacelle yielding a kind of TORA, where the mathematical model of new proposed TORA based barge-type OFWT is established by using Lagrange equations. Here, we have developed four disturbance observer (DO) based robust control algorithms for the proposed OFWT model stabilization and also present a comparative analysis of DO based backstepping sliding mode control, DO based backstepping integral sliding mode control, DO based backstepping nonsingular terminal sliding mode control, and DO based new backstepping integral nonsingular terminal sliding mode control techniques. Through theoretically and MATLAB simulations, we have verified the correctness of the proposed OFWT model and control techniques. This new TORA based barge-type OFWT model and the use of DO based new backstepping integral nonsingular terminal sliding mode control, has differentiate this work with the previous research work.

The rest of the paper includes the following headings which are: Dynamics of TORA based barge-type OFWT, Disturbance observer based robust control design techniques in which Finite-time nonlinear DO, DO based BSMC, DO based BISMC, DO based BNTSMC, and
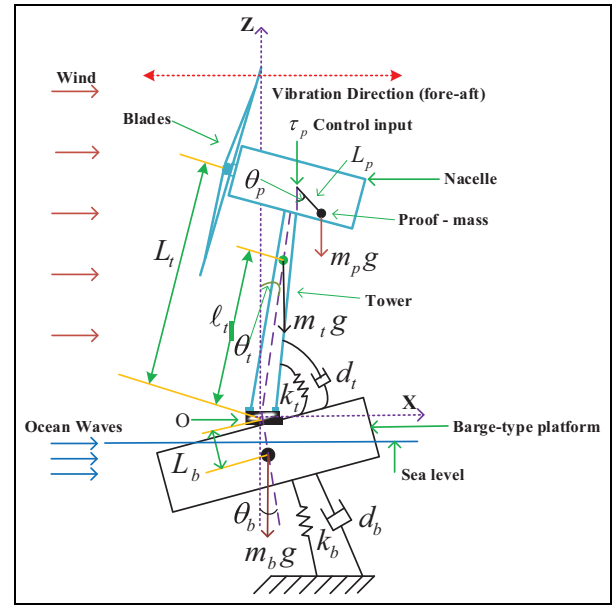

Figure 2. TORA based barge-type OFWT model.

DO based BINTSMC are included, Simulation results with discussions and Conclusion respectively.

Dynamics of TORA based barge-type offshore floating wind turbine

This research work has taken a simplified model of National Renewable Energy Laboratory (NREL) 5-MW barge-type OFWT[16] with three-degree of freedom (3-DOF). The rigid bodies in the model consist of a barge-type platform ($40\,m \times 40m \times 10m$), tower (90m hub height), and a rotating proof-mass, which is placed outside the nacelle ($18m \times 6m \times 6m$) along the negative z-axis direction. In Figure 2, it can be seen that the oscillating body of OFWT is considered as TORA unactuated translating cart, while the addition of a proof-mass actuator in nacelle yields TORA active mass damper. This proposed model is based on 3-DOF motion, that is, pitch: the motion of the platform, fore-aft bending: the motion of tower, rotational movement of the proof-mass, and following assumptions:

Assumption 1[16]: It is assumed that the dynamics and DOF of the OFWT rotor, gearbox, and generator are not considered in this modeling.
Assumption 2[15,16]: The small-angle approximations are considered for the platform pitch motion and the tower fore-aft motion that they would not exceed 10° around its equilibrium position even in the heaviest wind and wave loading's.
Assumption 3: It is assumed that the proof-mass actuator would not exceed 90° from its normal equilibrium position (zero) due to the small-angle approximation of OFWT.

The tower is treated as a linear rigid rotating beam, which is hinged at origin "O". The origin O of the coordinate system xyz axes is located at the joint hinge

center of the tower and platform. The m_b is the mass of barge, having a moment of inertia I_b and L_b is the length from the joint hinge center to the center of the platform, while the constants: k_b, k_t and d_b, d_t represents the supporting spring stiffness and damping coefficient of the respective barge-type platform and tower. The m_t is the mass of the tower, having a moment of inertia I_t and L_t is the length of the tower from joint hinge center to the center of the nacelle, while ℓ_t is the distance from joint hinge to the tower center of mass and g is the gravitational force. The net mass of eccentric rotational proof-mass is $m_p = m_{p_1} + m_{p_2}$, where m_{p_1} is the mass of proof-mass and m_{p_2} is the mass of rod through which proof-mass is attached. This eccentric rotational proof-mass has a moment of inertia I_p about its center of mass, where its attached rod length is L_p from a point τ_p, while τ_p is the control input, applied to the proof-mass actuator. Let θ_b, θ_t, θ_p, and $\dot{\theta}_b$, $\dot{\theta}_t$, $\dot{\theta}_p$ shows the angular position and angular velocity of the barge platform, tower, and the rotational proof-mass actuator of the nacelle, respectively.

After thoroughly reviewing and grasping the working principle of TORA active mass damper control strategy and applying onto the OFWT, the mathematical model of TORA based barge-type floating wind turbine is derived by using Euler Lagrange equation of motion. Such that, the T_T is the total kinetic energy of the system and P_T is the total potential energy of the system, where the total kinetic energy T_T is a sum of kinetic energy (KE) of the barge-type floating platform T_{m_b}, KE of tower T_{m_t}, and KE of the rotational proof-mass actuator T_{m_p} as follows:

Kinetic Energy:

$$T_{m_b} = \frac{1}{2} I_b \dot{\theta}_b^2 \tag{1}$$

$$T_{m_t} = \frac{1}{2} I_t \dot{\theta}_t^2 \tag{2}$$

$$T_{m_p} = \frac{1}{2} m_p \left[\left(\frac{d}{dt}(L_t \sin\theta_t) + \frac{d}{dt}(L_p \sin\theta_p) \right)^2 \right.$$
$$\left. + \left(\frac{d}{dt}(L_t \cos\theta_t) + \frac{d}{dt}(L_p \cos\theta_p) \right)^2 \right] + \frac{1}{2} I_p \dot{\theta}_p^2$$
$$= \frac{1}{2} m_p L_t^2 \dot{\theta}_t^2 + \frac{1}{2} \left(m_p L_p^2 + I_p \right) \dot{\theta}_p^2$$
$$+ m_p L_t L_p \dot{\theta}_t \dot{\theta}_p \cos(\theta_t - \theta_p) \tag{3}$$

The total KE can be written as

$$T_T = T_{m_b} + T_{m_t} + T_{m_p}$$
$$= \frac{1}{2} I_b \dot{\theta}_b^2 + \frac{1}{2} \left(m_p L_t^2 + I_t \right) \dot{\theta}_t^2 + \frac{1}{2} \left(m_p L_p^2 + I_p \right) \dot{\theta}_p^2$$
$$+ m_p L_t L_p \dot{\theta}_t \dot{\theta}_p \cos(\theta_t - \theta_p) \tag{4}$$

Similarly, the total potential energy P_T is a sum of potential energy (PE) of the barge-type floating platform P_{m_b}, PE of tower P_{m_t}, and PE of the rotational proof-mass actuator P_{m_p} as follows:

Potential Energy:

$$P_{m_b} = \frac{1}{2} k_b \theta_b^2 - m_b g L_b \cos\theta_b \tag{5}$$

$$P_{m_t} = \frac{1}{2} k_t (\theta_t - \theta_b)^2 + m_t g \ell_t \cos\theta_t \tag{6}$$

$$P_{m_p} = m_p g (L_t \cos\theta_t - L_p \cos\theta_p) \tag{7}$$

The total PE can be written as

$$P_T = P_{m_b} + P_{m_t} + P_{m_p}$$
$$= \frac{1}{2} k_b \theta_b^2 + \frac{1}{2} k_t (\theta_t - \theta_b)^2 + m_t g \ell_t \cos\theta_t$$
$$- m_b g L_b \cos\theta_b + m_p g (L_t \cos\theta_t - L_p \cos\theta_p) \tag{8}$$

Thus, the Lagrangian of the system is given by

$$L = T_T - P_T$$
$$= \frac{1}{2} I_b \dot{\theta}_b^2 + \frac{1}{2} \left(m_p L_t^2 + I_t \right) \dot{\theta}_t^2 + \frac{1}{2} \left(m_p L_p^2 + I_p \right) \dot{\theta}_p^2$$
$$+ m_p L_t L_p \dot{\theta}_t \dot{\theta}_p \cos(\theta_t - \theta_p) - \frac{1}{2} k_b \theta_b^2$$
$$- \frac{1}{2} k_t (\theta_t - \theta_b)^2 + m_b g L_b \cos\theta_b$$
$$- (m_p L_t + m_t \ell_t) g \cos\theta_t + m_p g L_p \cos\theta_p \tag{9}$$

The Euler-Lagrange equations of motion for the proposed TORA based barge-type floating wind turbine model can be written as

$$\frac{d}{dt} \left(\frac{\partial}{\partial \dot{\theta}_b}(L) \right) - \frac{\partial}{\partial \theta_b}(L) = Q_{\theta_b} \tag{10}$$

$$\frac{d}{dt} \left(\frac{\partial}{\partial \dot{\theta}_t}(L) \right) - \frac{\partial}{\partial \theta_t}(L) = Q_{\theta_t} \tag{11}$$

$$\frac{d}{dt} \left(\frac{\partial}{\partial \dot{\theta}_p}(L) \right) - \frac{\partial}{\partial \theta_p}(L) = \tau_p \tag{12}$$

where τ_p is the control input and Q_{θ_b}, Q_{θ_t} are the non-potential forces of the platform and tower, as follows:

$$Q_{\theta_b} = -d_t \dot{\theta}_b + d_t \dot{\theta}_t - d_b \dot{\theta}_b$$
$$Q_{\theta_t} = d_t \dot{\theta}_b - d_t \dot{\theta}_t$$

So, after solving the Euler-Lagrange equations of motion for TORA based barge-type floating wind turbine model, we have achieved the following dynamics

$$\begin{cases} I_b \ddot{\theta}_b + d_b \dot{\theta}_b - d_t (\dot{\theta}_t - \dot{\theta}_b) + m_b g L_b \sin\theta_b + k_b \theta_b \\ \quad -k_t (\theta_t - \theta_b) = 0 \\ (m_p L_t^2 + I_t) \ddot{\theta}_t + m_p L_t L_p \cos(\theta_t - \theta_p) \ddot{\theta}_p \\ \quad + m_p L_t L_p \sin(\theta_t - \theta_p) \dot{\theta}_p^2 + d_t (\dot{\theta}_t - \dot{\theta}_b) \\ \quad -(m_p L_t + m_t \ell_t) g \sin\theta_t + k_t (\theta_t - \theta_b) = 0 \\ (m_p L_p^2 + I_p) \ddot{\theta}_p + m_p L_t L_p \cos(\theta_t - \theta_p) \ddot{\theta}_t \\ \quad -L_t L_p m_p \sin(\theta_t - \theta_p) \dot{\theta}_t^2 + g L_p m_p \sin\theta_p = \tau_p \end{cases} \tag{13}$$

The equation (13) can be represented in a compact form as follows:

$$M(\wp)\ddot{\wp} + C(\wp,\dot{\wp})\dot{\wp} + G(\wp) = U_c \tag{14}$$

where

$$\wp = \begin{bmatrix} \theta_b & \theta_t & \theta_p \end{bmatrix}^T,$$

$$M(\wp) = \begin{bmatrix} h_0 & 0 & 0 \\ 0 & h_2 & h_7 \\ 0 & h_7 & h_5 \end{bmatrix},$$

$$C(\wp,\dot{\wp}) = \begin{bmatrix} d_b + d_t & -d_t & 0 \\ -d_t & d_t & h_8\dot{\theta}_p \\ 0 & -h_8\dot{\theta}_t & 0 \end{bmatrix},$$

$$G(\wp) = \begin{bmatrix} h_t \sin\theta_b + k_b\theta_b - k_t(\theta_t - \theta_b) \\ -h_4 \sin\theta_t + k_t(\theta_t - \theta_b) \\ h_6 \sin\theta_p \end{bmatrix},$$

$$U_c = \begin{bmatrix} 0 \\ 0 \\ \tau_p \end{bmatrix}.$$

The following constant parameters used in a compact form are: k_b, k_t, d_b, d_t, $h_0 = I_b$, $h_1 = m_b g L_b$, $h_2 = (m_p L_t^2 + I_t)$, $h_3 = m_p L_t L_p$, $h_4 = (m_p L_t + m_t \ell_t)g$, $h_5 = m_p L_p^2 + I_p$, $h_6 = m_p g L_p$, where we can further define: $h_7 = h_3 \cos(\theta_t - \theta_p)$, $h_8 = h_3 \sin(\theta_t - \theta_p)$.

The Table 1 presents the value of different constant parameters, which are mostly chosen from reference paper[16] due to the same structure of barge-type OFWT. The small-angle approximation for platform and tower are defined as: $\sin\theta_b = \theta_b$, $\sin\theta_t = \theta_t$, $\cos\theta_b = 1$, and $\cos\theta_t = 1$. In the compact form (14), $\wp$ is the configuration variable vector of the proposed TORA based barge-type OFWT system, the actuated variable θ_p is the angular position of the proof-mass, and two unactuated variables θ_b, θ_t are the angular position of the barge-type platform and tower respectively. Since there is only one actuated configuration variable that can control all the three configuration variables, hence, the proposed OFWT system is an underactuated system. Here, $M(\wp)$ is the inertia matrix, $C(\wp,\dot{\wp})$ shows the Coriolis and centrifugal force matrix, $G(\wp)$ is the potential energy matrix and U_c is the control input vector, respectively.

By assuming the proposed OFWT system states as $x = \begin{bmatrix} x_a & x_b & x_c & x_d & x_e & x_f \end{bmatrix}^T = \begin{bmatrix} \theta_b & \dot{\theta}_b & \theta_t & \dot{\theta}_t & \theta_p & \dot{\theta}_p \end{bmatrix}^T$, we can rewrite our proposed OFWT model (13) into a general affine form, such as

$$\dot{x} = p(x) + q(x)u \tag{15}$$

we have

$$p(x) = \begin{bmatrix} x_b \\ p_1(x) \\ x_d \\ p_2(x) \\ x_f \\ p_3(x) \end{bmatrix}, \quad q(x) = \begin{bmatrix} 0 \\ q_1(x) \\ 0 \\ q_2(x) \\ 0 \\ q_3(x) \end{bmatrix}, \quad u = \tau_p.$$

Table 1. TORA based barge-type offshore floating wind turbine parameters.

Parameter (Units)	Value	Description
m_b(kg)	61,50,000	Platform mass.
m_t(kg)	3,47,460	Tower mass.
m_N(kg)	3,50,000	Nacelle mass.
m_{p_1}(kg)	84,000	Mass of proof-mass.
m_{p_2}(kg)	42,000	Mass of proof-mass rod.
L_t(m)	90	Tower length.
L_p(m)	6	Proof-mass rod length.
$(L_b$(m), 0, ℓ_t(m))	(−0.28, 0, 64)	Overall center of mass.
I_b(kg × m^2)	1,69,45,00,000	Platform inertia.
I_t(kg × m^2)	1,82,17,00,000	Tower inertia.
I_p(kg × m^2)	35,28,000	Inertia of proof-mass rotor.
k_b(N/ m)	14,17,10,00,000	Spring stiffness of platform.
k_t(N/ m)	97,99,00,00,000	Spring stiffness of tower.
d_b(N× s / m)	3,63,74,00,000	Platform damping coefficient.
d_t(N× s / m)	2,10,32,00,000	Tower damping coefficient.
g(m / s^2)	9.81	Gravitational acceleration constant.

where

$$p_1(x) = \frac{p_1}{\det(M)}, \quad p_2(x) = \frac{p_2}{\det(M)}, \quad p_3(x) = \frac{p_3}{\det(M)},$$

$$q_1(x) = \frac{q_1}{\det(M)}, \quad q_2(x) = \frac{q_2}{\det(M)}, \quad q_3(x) = \frac{q_3}{\det(M)},$$

$$p_1 = \{-(k_b + k_t + h_1)x_a - (d_b + d_t)x_b + k_t x_c + d_t x_d\} \times \{h_2 h_5 - h_3^2 \cos^2(x_c - x_e)\},$$

$$q_1 = 0,$$

$$p_2 = h_0 h_5 \{-h_3 \sin(x_c - x_e)x_f^2 + k_t x_a. + (h_4 - k_t)x_c + d_t x_b - d_t x_d\} - h_0 h_3 \cos(x_c - x_e)\{-h_6 \sin x_e + h_3 \sin(x_c - x_e)x_d^2\},$$

$$q_2 = -h_0 h_3 \cos(x_c - x_e),$$

$$p_3 = h_0 h_2 \{h_3 \sin(x_c - x_e)x_d^2 - h_6 \sin x_e\} - h_0 h_3 \cos(x_c - x_e)\{-h_3 \sin(x_c - x_e)x_f^2. + k_t x_a + d_t x_b + (h_4 - k_t)x_c - d_t x_d\},$$

$$q_3 = h_0 h_2,$$

$$\det(M) = h_0 h_2 h_5 - h_0 h_3^2 \cos^2(x_c - x_e) > 0.$$

To get equilibrium points of the proposed OFWT model, let $u = 0$ and $p(x) = 0$. Thus, $x_b = x_d = x_f = 0$, then $p_1 = 0$, $p_2 = 0$, and $p_3 = 0$. By using this information, we can further simplify it, as follows:

$$\{-(k_b + k_t + h_1)x_a + k_t x_c\}\{h_2 h_5 - h_3^2 \cos^2(x_c - x_e)\} = 0 \tag{16}$$

$$h_0 h_5 \{k_t x_a + (h_4 - k_t)x_c\} + h_0 h_3 h_6 \cos(x_c - x_e)\sin x_e = 0 \tag{17}$$

$$- h_0 h_2 h_6 \sin x_e - h_0 h_3 \cos(x_c - x_e)$$
$$\{k_t x_a + (h_4 - k_t) x_c\} = 0 \tag{18}$$

Thus, we have $x_a = 0$, $x_c = 0$ and $x_e = \theta_e$, where $\theta_e = n\pi$ and $n = 0, \pm 1, \pm 2, \ldots$ such as

$$x_{eq} = [0, 0, 0, 0, \theta_e, 0]^T, \; \theta_e = n\pi, \; n = 0, \pm 1, \pm 2, \ldots \tag{19}$$

The equation (19) shows the equilibrium points of the proposed OFWT model. As in this paper, we assumed that the proof-mass actuator would not exceed 90° from its normal equilibrium point "0", hence, here we only consider the equilibrium point $\theta_e = 0$ and design different control laws for the stabilization of the proposed OFWT.

DO based robust control design techniques

In this section, disturbance observer (DO) and four DO based robust control design techniques, which are: DO based backstepping sliding mode control (DOBBSMC), DO based backstepping integral sliding mode control (DOBBISMC), DO based backstepping nonsingular terminal sliding mode control (DOBBNTSMC), and DO based backstepping integral nonsingular terminal sliding mode control (DOBBINTSMC) are implemented for the stabilization of OFWT.

Finite-time nonlinear disturbance observer

The general affine form (15) of OFWT with an addition of bounded disturbance $\psi(t)$, such that $\psi^* = \sup|\psi(t)|$ for $t > 0$ can be written as follows:

$$\dot{x} = p(x) + q(x)u + \psi(t) \tag{20}$$

In Shtessel et al.[37] and Li et al.,[38] a finite-time nonlinear disturbance observer is designed for such systems (20) with the consideration that disturbance is jth differentiable and have a Lipshitz constant $\hbar > 0$ for $\psi^j(t)$, as follows:

$$\begin{cases} \dot{\lambda}_0 = \dagger_0 + \dot{x}, \; \dot{\lambda}_1 = \dagger_1, \; \ldots, \; \dot{\lambda}_{j-1} = \dagger_{j-1}, \; \dot{\lambda}_j = \dagger_j, \\ \dagger_0 = -\Delta_0 \hbar^{1/(j+1)} |\lambda_0 - x|^{j/(j+1)} \operatorname{sgn}(\lambda_0 - x) + \lambda_1, \\ \dagger_1 = -\Delta_1 \hbar^{1/j} |\lambda_1 - \dagger_0|^{(j-1)/j} \operatorname{sgn}(\lambda_1 - \dagger_0) + \lambda_2, \\ \vdots \\ \dagger_{j-1} = -\Delta_{j-1} \hbar^{1/2} |\lambda_{j-1} - \dagger_{j-2}|^{1/2} \operatorname{sgn}(\lambda_{j-1} - \dagger_{j-2}) \\ \qquad + \lambda_j, \\ \dagger_j = -\Delta_j \hbar \operatorname{sgn}(\lambda_j - \dagger_{j-1}), \end{cases} \tag{21}$$

where $\Delta_i > 0$ ($i = 0, 1, \ldots, j$) is the observer design constants and $\hat{\psi}(t) = \lambda_1$ is the estimated disturbance. The observer/differentiator estimation error stability can be achieved by combining (20) with (21), as follows:

$$\begin{cases} \dot{\xi}_0 = -\Delta_0 \hbar^{1/(j+1)} |\xi_0|^{j/(j+1)} \operatorname{sgn}(\xi_0) + \xi_1, \\ \dot{\xi}_1 = -\Delta_1 \hbar^{1/j} |\xi_1 - \dot{\xi}_0|^{(j-1)/j} \operatorname{sgn}(\xi_1 - \dot{\xi}_0) + \xi_2, \\ \vdots \\ \dot{\xi}_{j-1} = -\Delta_{j-1} \hbar^{1/2} |\xi_{j-1} - \dot{\xi}_{j-2}|^{1/2} \operatorname{sgn}(\xi_{j-1} - \dot{\xi}_{j-2}) \\ \qquad + \xi_j, \\ \dot{\xi}_j \in -\Delta_j \hbar \operatorname{sgn}(\xi_j - \dot{\xi}_{j-1}) + [-\hbar, \; \hbar] \end{cases} \tag{22}$$

where, finite-time estimation error is $\xi = \lambda_1 - \psi(t) = 0$ for $t \geq t_f$. Now, for achieving hierarchical DO based sliding mode control scheme, the general affine form of OFWT (20) can be written into three decomposed second-order nonlinear subsystems along with unknown mismatched bounded disturbance $\psi_b(t)$, $\psi_t(t)$, and $\psi_p(t)$, as follows:

$$\begin{cases} \begin{cases} \dot{x}_a = x_b + \psi_b(t) \\ \dot{x}_b = p_1(x) \end{cases} \\ \begin{cases} \dot{x}_c = x_d + \psi_t(t) \\ \dot{x}_d = p_2(x) + q_2(x)u \end{cases} \\ \begin{cases} \dot{x}_e = x_f + \psi_p(t) \\ \dot{x}_f = p_3(x) + q_3(x)u \end{cases} \end{cases} \tag{23}$$

These three second-order nonlinear subsystems consist of state variables (x_a, x_b), (x_c, x_d), and (x_e, x_f), respectively. The estimated disturbance of $\psi_b(t)$, $\psi_t(t)$, and $\psi_p(t)$ for subsystem (23) can be obtained, as follows:

$$\begin{cases} \dot{\lambda}_0 = \dagger_0 + x_b, \; \dot{\lambda}_1 = \dagger_1, \; \dot{\lambda}_2 = \dagger_2, \\ \dagger_0 = -\Delta_0 \hbar^{1/3} |\lambda_0 - x_a|^{2/3} \operatorname{sgn}(\lambda_0 - x_a) + \lambda_1, \\ \dagger_1 = -\Delta_1 \hbar^{1/2} |\lambda_1 - \dagger_0|^{1/2} \operatorname{sgn}(\lambda_1 - \dagger_0) + \lambda_2, \\ \dagger_2 = -\Delta_2 \hbar \operatorname{sgn}(\lambda_2 - \dagger_1) \end{cases} \tag{24}$$

$$\begin{cases} \dot{\lambda}_3 = \dagger_3 + x_d, \; \dot{\lambda}_4 = \dagger_4, \; \dot{\lambda}_5 = \dagger_5, \\ \dagger_3 = -\Delta_3 \hbar^{1/3} |\lambda_3 - x_c|^{2/3} \operatorname{sgn}(\lambda_3 - x_c) + \lambda_4, \\ \dagger_4 = -\Delta_4 \hbar^{1/2} |\lambda_4 - \dagger_3|^{1/2} \operatorname{sgn}(\lambda_4 - \dagger_3) + \lambda_5, \\ \dagger_5 = -\Delta_5 \hbar \operatorname{sgn}(\lambda_5 - \dagger_4) \end{cases} \tag{25}$$

$$\begin{cases} \dot{\lambda}_6 = \dagger_6 + x_f, \; \dot{\lambda}_7 = \dagger_7, \; \dot{\lambda}_8 = \dagger_8, \\ \dagger_6 = -\Delta_6 \hbar^{1/3} |\lambda_6 - x_e|^{2/3} \operatorname{sgn}(\lambda_6 - x_e) + \lambda_7, \\ \dagger_7 = -\Delta_7 \hbar^{1/2} |\lambda_7 - \dagger_6|^{1/2} \operatorname{sgn}(\lambda_7 - \dagger_6) + \lambda_8, \\ \dagger_8 = -\Delta_8 \hbar \operatorname{sgn}(\lambda_8 - \dagger_7) \end{cases} \tag{26}$$

where λ_1, λ_4, and λ_7 are the estimated disturbances of $\psi_b(t)$, $\psi_t(t)$, and $\psi_p(t)$ respectively. Through following the backstepping[31] procedure along with using

respective finite time estimated disturbance, all these three second-order subsystems of OFWT can be converted into a new three backstepped second-order nonlinear subsystems. Then, disturbance observer based four robust switching control law (DOBBSMC, DOBBISMC, DOBBNTSMC, and DOBBINTSMC) will be designed by using these three backstepped second-order nonlinear subsystems. Now, for obtaining three DO based backstepped second-order nonlinear subsystems of OFWT from equation (23), we can define a new state variable for the first subsystem as follows:

$$Y_1 = x_a \tag{27}$$

A Lyapunov candidate can be defined as

$$V(Y_1) = \frac{1}{2}Y_1^2 \tag{28}$$

Taking time derivative and simplifying yields

$$\dot{V}(Y_1) = Y_1\dot{Y}_1 = Y_1(x_b + \psi_b(t)) \tag{29}$$

For the stability of Y_1, a virtual control input of x_b is introduced as follows:

$$x_b = -\Gamma_1 Y_1 - \lambda_1 \tag{30}$$

where Γ_1 is a positive constant. Now, invoking the virtual control input in (29) yields

$$\dot{V}(Y_1) = -\Gamma_1 Y_1^2 - Y_1\xi_b \tag{31}$$

Therefore, with the design of $\Gamma_1 > 0$ results a stable dynamics for Y_1. Here ξ_b represents the finite time disturbance error for barge of OFWT , that is $\xi_b = \lambda_1 - \psi_b(t)$. Now, to change the variable and backstep, from (30), we can write

$$Y_2 = x_b + \Gamma_1 Y_1 + \lambda_1 \tag{32}$$

Hence, the first second-order state space model of OFWT can be extracted based on back-stepped variables as follows:

$$\begin{cases} \dot{Y}_1 = Y_2 - \Gamma_1 Y_1 - \xi_b \\ \dot{Y}_2 = p_1(x) + \Gamma_1(Y_2 - \Gamma_1 Y_1 - \xi_b) + \dagger_1 \end{cases} \tag{33}$$

Similarly, with the same procedure, the remaining two second-order state space model of OFWT can be obtained by selecting variable $Y_3 = x_c$, $Y_5 = x_e$ and defining Lyapunov candidate $V(Y_3) = \frac{1}{2}Y_3^2$, $V(Y_5) = \frac{1}{2}Y_5^2$ where, $Y_4 = x_d + \Gamma_2 Y_3 + \lambda_4$, $Y_6 = x_f + \Gamma_3 Y_5 + \lambda_7$ respectively, as follows:

$$\begin{cases} \dot{Y}_3 = Y_4 - \Gamma_2 Y_3 - \xi_t \\ \dot{Y}_4 = p_2(x) + q_2(x)u + \Gamma_2(Y_4 - \Gamma_2 Y_3 - \xi_t) + \dagger_4 \end{cases} \tag{34}$$

and

$$\begin{cases} \dot{Y}_5 = Y_6 - \Gamma_3 Y_5 - \xi_p \\ \dot{Y}_6 = p_3(x) + q_3(x)u + \Gamma_3(Y_6 - \Gamma_3 Y_5 - \xi_p) + \dagger_7 \end{cases} \tag{35}$$

where Γ_2, Γ_3 are the positive design constants and ξ_t, ξ_p represents the finite time disturbance error for tower and proof-mass actuator of OFWT respectively, such as $\xi_t = \lambda_4 - \psi_t(t)$, $\xi_p = \lambda_7 - \psi_p(t)$. By using equations (33)–(35), we can derive DO based backstepping sliding mode control schemes.

DO based backstepping sliding mode control

In industry and academia, a Lyapunov-based sliding mode control is a well known robust control method for nonlinear systems. Backstepping is another nonlinear control technique, which requires accurate modeling information, while SMC has a robust property for system uncertain parameters. Through following the Lyapunov stability theory, sliding mode control develop a switching control law, which converges the system forcefully to the sliding surface while trapping the system within a boundary layer near the sliding surface. To enhance the robustness of SMC, we have designed a disturbance observer-based backstepping hierarchical sliding mode control algorithm. For this, we can choose three sub-sliding mode surfaces corresponding to the three backstepped subsystems (33)–(35) respectively, as follows:

$$\zeta_1 = \sigma_a Y_1 + \sigma_b Y_2 \tag{36}$$
$$\zeta_2 = \sigma_c Y_3 + \sigma_d Y_4 \tag{37}$$
$$\zeta_3 = \sigma_e Y_5 + \sigma_f Y_6 \tag{38}$$

where $\sigma_a, \sigma_b, \sigma_c, \sigma_d, \sigma_e,$ and σ_f are the positive sliding mode surface control parameters. Through hierarchical sliding mode control method,[29] we can take total sliding mode surface and its derivative as follows:

$$\zeta_T = \zeta_1 + \zeta_2 + \zeta_3 \tag{39}$$
$$\dot{\zeta}_T = \dot{\zeta}_1 + \dot{\zeta}_2 + \dot{\zeta}_3 \tag{40}$$

where

$$\dot{\zeta}_1 = \sigma_a(Y_2 - \Gamma_1 Y_1 - \xi_b) + \sigma_b(p_1(x) + \Gamma_1(Y_2 - \Gamma_1 Y_1 - \xi_b) + \dagger_1)$$

$$\dot{\zeta}_2 = \sigma_c(Y_4 - \Gamma_2 Y_3 - \xi_t) + \sigma_d(p_2(x) + q_2(x)u + \Gamma_2(Y_4 - \Gamma_2 Y_3 - \xi_t) + \dagger_4)$$

$$\dot{\zeta}_3 = \sigma_e(Y_6 - \Gamma_3 Y_5 - \xi_p) + \sigma_f(p_3(x) + q_3(x)u + \Gamma_3(Y_6 - \Gamma_3 Y_5 - \xi_p) + \dagger_7)$$

For the convergence of total sliding mode surface toward zero, according to sliding mode theory, the surface ζ_T based Lyapunov candidate can be defined, as follows:

$$V_T = (0.5)\zeta_T^2 \tag{41}$$

Taking time derivative of Lyapunov candidate (41) and further simplifying yields

$$
\begin{aligned}
\dot{V}_T &= \zeta_T \dot{\zeta}_T \\
&= \zeta_T [\sigma_a(\Upsilon_2 - \Gamma_1\Upsilon_1 - \xi_b) + \sigma_c(\Upsilon_4 - \Gamma_2\Upsilon_3 - \xi_t) \\
&\quad + \sigma_e(\Upsilon_6 - \Gamma_3\Upsilon_5 - \xi_p) + \sigma_b(p_1(x) + \Gamma_1(\Upsilon_2 - \Gamma_1\Upsilon_1 \\
&\quad - \xi_b) + \dagger_1) + \sigma_d(p_2(x) + \Gamma_2(\Upsilon_4 - \Gamma_2\Upsilon_3 - \xi_t) + \dagger_4) \\
&\quad + \sigma_f(p_3(x) + \Gamma_3(\Upsilon_6 - \Gamma_3\Upsilon_5 - \xi_p) + \dagger_7) \\
&\quad + (\sigma_d q_2(x) + \sigma_f q_3(x))u]
\end{aligned}
\tag{42}
$$

Hence, the backstepping sliding mode control law can be chosen as

$$
\begin{aligned}
u &= -\frac{1}{\sigma_d q_2(x) + \sigma_f q_3(x)} \\
&\quad [\sigma_a(\Upsilon_2 - \Gamma_1\Upsilon_1) + \sigma_c(\Upsilon_4 - \Gamma_2\Upsilon_3) \\
&\quad + \sigma_e(\Upsilon_6 - \Gamma_3\Upsilon_5) + \sigma_b(p_1(x) + \Gamma_1(\Upsilon_2 - \Gamma_1\Upsilon_1) \\
&\quad + \dagger_1) + \sigma_d(p_2(x) + \Gamma_2(\Upsilon_4 - \Gamma_2\Upsilon_3) + \dagger_4) \\
&\quad + \sigma_f(p_3(x) + \Gamma_3(\Upsilon_6 - \Gamma_3\Upsilon_5) + \dagger_7) + \varpi \cdot \text{sgn}(\zeta_T) \\
&\quad + \alpha \cdot \zeta_T]
\end{aligned}
\tag{43}
$$

where $\varpi > 0$ and $\alpha > 0$ are the gain constants. Now, substituting u in equation (42) yields

$$
\begin{aligned}
\dot{V}_T &= \zeta_T [-(\sigma_a + \sigma_b)\xi_b - (\sigma_c + \sigma_d)\xi_t - (\sigma_e + \sigma_f)\xi_p \\
&\quad - \varpi \cdot \text{sgn}(\zeta_T) - \alpha \cdot \zeta_T] \\
&\leqslant -(\sigma_a + \sigma_b)\eta_b\zeta_T - (\sigma_c + \sigma_d)\eta_t\zeta_T - (\sigma_e + \sigma_f)\eta_p\zeta_T \\
&\quad - \varpi \cdot |\zeta_T| - \alpha \cdot \zeta_T^2
\end{aligned}
\tag{44}
$$

Since the finite-time DO error system (22) is stable and the estimated disturbance error is bounded by $|\xi_b| \leqslant \eta_b$, $|\xi_t| \leqslant \eta_t$, and $|\xi_p| \leqslant \eta_p$, where $\eta_b > 0$, $\eta_t > 0$, and $\eta_p > 0$. Hence, finite-time disturbance observer must have a quick stable dynamic than the control scheme. In (44), the derivative of Lyapunov candidate is negative definite, which means that the total sliding surface is Lyapunov stable and the system dynamics will converge to zero asymptotically.

DO based backstepping integral sliding mode control

According to ISMC theory, some of the small perturbations and uncertainties show very sensitive behavior into the SMC reaching phase of the nonlinear systems, which generates undesirable results or even destabilize the system. Thus, a free reaching phase sliding mode surface was needed. To overcome this issue, an integral term is preferred to include in the sliding manifold which gives the guarantee of eliminated reaching phase. For achieving further robustness of ISMC, we have designed a disturbance observer-based backstepping hierarchical integral sliding mode control algorithm. In DO based BISMC case, the same procedure will be repeated as like DO based BSMC. Three integral based sub-sliding mode surfaces can be chosen from equations (33)–(35), as follows:

$$\zeta_1 = \sigma_a\Upsilon_1 + \sigma_b\Upsilon_2 + \sigma_g \int \Upsilon_1 \tag{45}$$

$$\zeta_2 = \sigma_c\Upsilon_3 + \sigma_d\Upsilon_4 + \sigma_h \int \Upsilon_3 \tag{46}$$

$$\zeta_3 = \sigma_e\Upsilon_5 + \sigma_f\Upsilon_6 + \sigma_i \int \Upsilon_5 \tag{47}$$

where $\sigma_a, \sigma_b, \sigma_c, \sigma_d, \sigma_e, \sigma_f, \sigma_g, \sigma_h,$ and σ_i are the positive backstepping integral sliding mode surface control parameters. The total backstepping integral sliding mode surface can be taken as

$$\zeta_T = \zeta_1 + \zeta_2 + \zeta_3 \tag{48}$$

$$\dot{\zeta}_T = \dot{\zeta}_1 + \dot{\zeta}_2 + \dot{\zeta}_3 \tag{49}$$

where

$$
\begin{aligned}
\dot{\zeta}_1 &= \sigma_a(\Upsilon_2 - \Gamma_1\Upsilon_1 - \xi_b) + \sigma_b(p_1(x) + \Gamma_1(\Upsilon_2 \\
&\quad - \Gamma_1\Upsilon_1 - \xi_b) + \dagger_1) + \sigma_g\Upsilon_1 \\
\dot{\zeta}_2 &= \sigma_c(\Upsilon_4 - \Gamma_2\Upsilon_3 - \xi_t) + \sigma_d(p_2(x) + q_2(x)u \\
&\quad + \Gamma_2(\Upsilon_4 - \Gamma_2\Upsilon_3 - \xi_t) + \dagger_4) + \sigma_h\Upsilon_3 \\
\dot{\zeta}_3 &= \sigma_e(\Upsilon_6 - \Gamma_3\Upsilon_5 - \xi_p) + \sigma_f(p_3(x) + q_3(x)u \\
&\quad + \Gamma_3(\Upsilon_6 - \Gamma_3\Upsilon_5 - \xi_p) + \dagger_7) + \sigma_i\Upsilon_5
\end{aligned}
$$

Defining a Lyapunov candidate based on surface ζ_T, as follows:

$$V_T = (0.5)\zeta_T^2 \tag{50}$$

Taking time derivative of Lyapunov candidate (50) and further simplifying yields

$$
\begin{aligned}
\dot{V}_T &= \zeta_T \dot{\zeta}_T \\
&= \zeta_T [\sigma_a(\Upsilon_2 - \Gamma_1\Upsilon_1 - \xi_b) + \sigma_c(\Upsilon_4 - \Gamma_2\Upsilon_3 - \xi_t) \\
&\quad + \sigma_e(\Upsilon_6 - \Gamma_3\Upsilon_5 - \xi_p) + \sigma_b(p_1(x) + \Gamma_1(\Upsilon_2 - \Gamma_1\Upsilon_1 \\
&\quad - \xi_b) + \dagger_1) + \sigma_d(p_2(x) + \Gamma_2(\Upsilon_4 - \Gamma_2\Upsilon_3 - \xi_t) + \dagger_4) \\
&\quad + \sigma_f(p_3(x) + \Gamma_3(\Upsilon_6 - \Gamma_3\Upsilon_5 - \xi_p) + \dagger_7) + \sigma_g\Upsilon_1 \\
&\quad + \sigma_h\Upsilon_3 + \sigma_i\Upsilon_5 + (\sigma_d q_2(x) + \sigma_f q_3(x))u]
\end{aligned}
\tag{51}
$$

From equation (51), we can choose backstepping integral sliding mode control as follows:

$$u = -\frac{1}{\sigma_d q_2(x) + \sigma_f q_3(x)}[\sigma_a(Y_2 - \Gamma_1 Y_1) + \sigma_c(Y_4 - \Gamma_2 Y_3)$$
$$+ \sigma_e(Y_6 - \Gamma_3 Y_5) + \sigma_b(p_1(x) + \Gamma_1(Y_2 - \Gamma_1 Y_1)$$
$$+ \dagger_1) + \sigma_d(p_2(x) + \Gamma_2(Y_4 - \Gamma_2 Y_3) + \dagger_4) + \sigma_g Y_1$$
$$+ \sigma_f(p_3(x) + \Gamma_3(Y_6 - \Gamma_3 Y_5) + \dagger_7) + \sigma_h Y_3 + \sigma_i Y_5$$
$$+ \varpi \cdot \mathrm{sgn}(\zeta_T) + \alpha \cdot \zeta_T] \tag{52}$$

where $\varpi > 0$ and $\alpha > 0$ are the gain constants. Now, substituting u in equation (51) yields

$$\dot{V}_T = \zeta_T[-(\sigma_a + \sigma_b)\xi_b - (\sigma_c + \sigma_d)\xi_t - (\sigma_e + \sigma_f)\xi_p$$
$$-\varpi \cdot \mathrm{sgn}(\zeta_T) - \alpha \cdot \zeta_T]$$
$$\leqslant -(\sigma_a + \sigma_b)\eta_b \zeta_T - (\sigma_c + \sigma_d)\eta_t \zeta_T - (\sigma_e + \sigma_f)\eta_p \zeta_T$$
$$-\varpi \cdot |\zeta_T| - \alpha \cdot \zeta_T^2 \tag{53}$$

where $\eta_b > 0$, $\eta_t > 0$, and $\eta_p > 0$ for finite-time bounded estimated disturbance error $|\xi_b| \leqslant \eta_b$, $|\xi_t| \leqslant \eta_t$, and $|\xi_p| \leqslant \eta_p$ respectively. In (53), the derivative of Lyapunov candidate is negative definite, which means that the total sliding surface is Lyapunov stable and the system dynamics will converge to zero asymptotically.

DO based backstepping nonsingular terminal sliding mode control

To provide the finite time states convergence of the nonlinear system without spending a large control effort is the characteristic of the terminal sliding mode control, while SMC and ISMC gives infinite time state convergence. A precise sliding mode surface is designed in TSMC and the role of control algorithm is to retain the system on the designed surface. In different nonlinear systems, by using TSMC, a singularity problem was occurred which can be resolved by following the nonsingular terminal sliding mode control (NTSMC) procedure in which a suitable fractional power is selected in sliding mode surface. To enhance the robustness of NTSMC, we have designed a disturbance observer-based backstepping hierarchical nonsingular terminal sliding mode control algorithm. The steps for designing DO based BNTSMC of OFWT is also same as like DOBBSMC, and DOBBISMC. Firstly, we have to choose three backstepping nonsingular terminal-based sub-sliding mode surfaces from equations (33)–(35), as follows:

$$\zeta_1 = \sigma_a Y_1 + \sigma_b Y_2 + \frac{1}{\varepsilon_1} Y_2^{\frac{v_1}{w_1}} \tag{54}$$

$$\zeta_2 = \sigma_c Y_3 + \sigma_d Y_4 + \frac{1}{\varepsilon_2} Y_4^{\frac{v_2}{w_2}} \tag{55}$$

$$\zeta_3 = \sigma_e Y_5 + \sigma_f Y_6 + \frac{1}{\varepsilon_3} Y_6^{\frac{v_3}{w_3}} \tag{56}$$

where $\sigma_a, \sigma_b, \sigma_c, \sigma_d, \sigma_e, \sigma_f, \varepsilon_1, \varepsilon_2$, and ε_3 are the positive control parameters of backstepping nonsingular terminal sliding mode surfaces, while v_1, w_1, v_2, w_2, v_3, and w_3

are the positive odd integers, which can be designed as $1 < \frac{v_1}{w_1} < 2$, $1 < \frac{v_2}{w_2} < 2$, and $1 < \frac{v_3}{w_3} < 2$. The total backstepping nonsingular terminal sliding mode surface can be taken as

$$\zeta_T = \zeta_1 + \zeta_2 + \zeta_3 \tag{57}$$

$$\dot{\zeta}_T = \dot{\zeta}_1 + \dot{\zeta}_2 + \dot{\zeta}_3 \tag{58}$$

where

$$\dot{\zeta}_1 = \sigma_a(Y_2 - \Gamma_1 Y_1 - \xi_b) + z_b(p_1(x) + \Gamma_1(Y_2 - \Gamma_1 Y_1 - \xi_b) + \dagger_1)$$

$$\dot{\zeta}_2 = \sigma_c(Y_4 - \Gamma_2 Y_3 - \xi_t) + z_t(p_2(x) + \Gamma_2(Y_4 - \Gamma_2 Y_3 - \xi_t) + \dagger_4) + z_t q_2(x)u$$

$$\dot{\zeta}_3 = \sigma_e(Y_6 - \Gamma_3 Y_5 - \xi_p) + z_p(p_3(x) + \Gamma_3(Y_6 - \Gamma_3 Y_5 - \xi_p) + \dagger_7) + z_p q_3(x)u$$

For simplicity, we have defined some parameters $J_1 = \frac{v_1}{\varepsilon_1 w_1}$, $J_2 = \frac{v_2}{\varepsilon_2 w_2}$, $J_3 = \frac{v_3}{\varepsilon_3 w_3}$, $z_1 = \frac{v_1}{w_1} - 1$, $z_2 = \frac{v_2}{w_2} - 1$, $z_3 = \frac{v_3}{w_3} - 1$, $z_b = \sigma_b + J_1 Y_2^{z_1}$, $z_t = \sigma_d + J_2 Y_4^{z_2}$, and $z_p = \sigma_f + J_3 Y_6^{z_3}$. Now, defining a Lyapunov candidate based on surface ζ_T as follows:

$$V_T = (0.5)\zeta_T^2 \tag{59}$$

Taking time derivative of Lyapunov candidate (59) and further simplifying yields

$$\dot{V}_T = \zeta_T \dot{\zeta}_T$$
$$= \zeta_T[\sigma_a(Y_2 - \Gamma_1 Y_1 - \xi_b) + \sigma_c(Y_4 - \Gamma_2 Y_3 - \xi_t)$$
$$+ \sigma_e(Y_6 - \Gamma_3 Y_5 - \xi_p) + z_b(p_1(x) + \Gamma_1(Y_2 - \Gamma_1 Y_1$$
$$- \xi_b) + \dagger_1) + z_t(p_2(x) + \Gamma_2(Y_4 - \Gamma_2 Y_3 - \xi_t) + \dagger_4)$$
$$+ z_p(p_3(x) + \Gamma_3(Y_6 - \Gamma_3 Y_5 - \xi_p) + \dagger_7) + (z_t q_2(x)$$
$$+ z_p q_3(x))u] \tag{60}$$

From equation (60), we can choose backstepping nonsingular terminal sliding mode control as follows:

$$u = -\frac{1}{z_t q_2(x) + z_p q_3(x)}[z_b(p_1(x) + \Gamma_1(Y_2 - \Gamma_1 Y_1) + \dagger_1)$$
$$+ \sigma_a(Y_2 - \Gamma_1 Y_1) + \sigma_c(Y_4 - \Gamma_2 Y_3) + \sigma_e(Y_6$$
$$- \Gamma_3 Y_5) + z_t(p_2(x) + \Gamma_2(Y_4 - \Gamma_2 Y_3) + \dagger_4)$$
$$+ z_p(p_3(x) + \Gamma_3(Y_6 - \Gamma_3 Y_5) + \dagger_7)$$
$$+ \varpi \cdot \mathrm{sgn}(\zeta_T)|\zeta_T|^\Xi + \alpha \cdot \zeta_T] \tag{61}$$

where $\varpi > 0$, $\alpha > 0$ are the gain constants and $0 < \Xi < 1$. Now, substituting u in equation (60) yields

$$\dot{V}_T = \zeta_T[-(\sigma_a + z_b)\xi_b - (\sigma_c + z_t)\xi_t - (\sigma_e + z_p)\xi_p$$
$$-\varpi \cdot \mathrm{sign}(\zeta_T)|\zeta_T|^\Xi - \alpha \cdot \zeta_T]$$
$$\leqslant -(\sigma_a + z_b)\eta_b \zeta_T - (\sigma_c + z_t)\eta_t \zeta_T - (\sigma_e + z_p)\eta_p \zeta_T$$
$$-\varpi \cdot |\zeta_T|^{\Xi+1} - \alpha \cdot \zeta_T^2 \tag{62}$$

where $\eta_b > 0$, $\eta_t > 0$, and $\eta_p > 0$ for finite-time bounded estimated disturbance error $|\xi_b| \leqslant \eta_b$, $|\xi_t| \leqslant \eta_t$, and $|\xi_p| \leqslant \eta_p$ respectively. In (62), the derivative of Lyapunov candidate is negative definite. From this, we can concluded that the total sliding surface is Lyapunov stable and it will not escape in finite time hence, the system dynamics will converge to zero in finite time.

DO based backstepping integral nonsingular terminal sliding mode control

The disturbance observer-based backstepping integral nonsingular terminal sliding mode control is a new modified form of disturbance observer-based backstepping nonsingular terminal sliding mode control. For designing such DO based BINTSMC technique, an integral of backstepping state is added into the proposed sliding surface for achieving fast finite time states stability as well as to improve chattering effect. From equations (33)–(35), three sub-sliding mode surfaces are chosen for the proposed DO based hierarchical BINTSMC, as follows:

$$\zeta_1 = \sigma_a Y_1 + \sigma_b Y_2 + \frac{1}{\varepsilon_1} Y_2^{\frac{v_1}{w_1}} + \sigma_g \int Y_1 \qquad (63)$$

$$\zeta_2 = \sigma_c Y_3 + \sigma_d Y_4 + \frac{1}{\varepsilon_2} Y_4^{\frac{v_2}{w_2}} + \sigma_h \int Y_3 \qquad (64)$$

$$\zeta_3 = \sigma_e Y_5 + \sigma_f Y_6 + \frac{1}{\varepsilon_3} Y_6^{\frac{v_3}{w_3}} + \sigma_i \int Y_5 \qquad (65)$$

where $\sigma_a, \sigma_b, \sigma_c, \sigma_d, \sigma_e, \sigma_f, \sigma_g, \sigma_h, \sigma_i, \varepsilon_1, \varepsilon_2$, and ε_3 are the positive control parameters of backstepping nonsingular integral terminal sliding mode surfaces, while v_1, w_1, v_2, w_2, v_3, and w_3 are the positive odd integers, which can be designed as $1 < \frac{v_1}{w_1} < 2$, $1 < \frac{v_2}{w_2} < 2$, and $1 < \frac{v_3}{w_3} < 2$. The total backstepping nonsingular integral terminal sliding mode surface can be taken as

$$\zeta_T = \zeta_1 + \zeta_2 + \zeta_3 \qquad (66)$$

$$\dot{\zeta}_T = \dot{\zeta}_1 + \dot{\zeta}_2 + \dot{\zeta}_3 \qquad (67)$$

where

$$\dot{\zeta}_1 = \sigma_a(Y_2 - \Gamma_1 Y_1 - \xi_b) + z_b(p_1(x) + \Gamma_1(Y_2 - \Gamma_1 Y_1 \\ - \xi_b) + \dagger_1) + \sigma_g Y_1$$

$$\dot{\zeta}_2 = \sigma_c(Y_4 - \Gamma_2 Y_3 - \xi_t) + z_t(p_2(x) + \Gamma_2(Y_4 - \Gamma_2 Y_3 \\ - \xi_t) + \dagger_4) + z_t q_2(x) u + \sigma_h Y_3$$

$$\dot{\zeta}_3 = \sigma_e(Y_6 - \Gamma_3 Y_5 - \xi_p) + z_p(p_3(x) + \Gamma_3(Y_6 - \Gamma_3 Y_5 \\ - \xi_p) + \dagger_7) + z_p q_3(x) u + \sigma_i Y_5$$

For simplicity, we have defined some parameters $J_1 = \frac{v_1}{\varepsilon_1 w_1}$, $J_2 = \frac{v_2}{\varepsilon_2 w_2}$, $J_3 = \frac{v_3}{\varepsilon_3 w_3}$, $z_1 = \frac{v_1}{w_1} - 1$, $z_2 = \frac{v_2}{w_2} - 1$, $z_3 = \frac{v_3}{w_3} - 1$, $z_b = \sigma_b + J_1 Y_2^{z_1}$, $z_t = \sigma_d + J_2 Y_4^{z_2}$, and $z_p = \sigma_f + J_3 Y_6^{z_3}$. Now, defining a Lyapunov candidate based on surface ζ_T as follows:

$$V_T = (0.5)\zeta_T^2 \qquad (68)$$

Taking time derivative of Lyapunov candidate (68) and further simplifying yields

$$\dot{V}_T = \zeta_T \dot{\zeta}_T \\ = \zeta_T[\sigma_a(Y_2 - \Gamma_1 Y_1 - \xi_b) + \sigma_c(Y_4 - \Gamma_2 Y_3 - \xi_t) \\ + \sigma_e(Y_6 - \Gamma_3 Y_5 - \xi_p) + z_b(p_1(x) + \Gamma_1(Y_2 - \Gamma_1 Y_1 \\ - \xi_b) + \dagger_1) + z_t(p_2(x) + \Gamma_2(Y_4 - \Gamma_2 Y_3 - \xi_t) + \dagger_4) \\ + z_p(p_3(x) + \Gamma_3(Y_6 - \Gamma_3 Y_5 - \xi_p) + \dagger_7) + \sigma_g Y_1 \\ + \sigma_h Y_3 + \sigma_i Y_5 + (z_t q_2(x) + z_p q_3(x))u] \qquad (69)$$

From equation (69), we can choose backstepping nonsingular integral terminal sliding mode control as follows:

$$u = -\frac{1}{z_t q_2(x) + z_p q_3(x)}[z_b(p_1(x) + \Gamma_1(Y_2 - \Gamma_1 Y_1) + \dagger_1) \\ + \sigma_a(Y_2 - \Gamma_1 Y_1) + \sigma_c(Y_4 - \Gamma_2 Y_3) + \sigma_e(Y_6 \\ - \Gamma_3 Y_5) + z_t(p_2(x) + \Gamma_2(Y_4 - \Gamma_2 Y_3) + \dagger_4) \\ + z_p(p_3(x) + \Gamma_3(Y_6 - \Gamma_3 Y_5) + \dagger_7) + \sigma_g Y_1 + \sigma_h Y_3 \\ + \sigma_i Y_5 + \varpi \cdot \text{sgn}(\zeta_T)|\zeta_T|^\Xi + \alpha \cdot \zeta_T] \qquad (70)$$

where $\varpi > 0$, $\alpha > 0$ are the gain constants and $0 < \Xi < 1$. Now, substituting u in equation (69) yields

$$\dot{V}_T = \zeta_T\big[-(\sigma_a + z_b)\xi_b - (\sigma_c + z_t)\xi_t - (\sigma_e + z_p)\xi_p \\ - \varpi \cdot \text{sgn}(\zeta_T)|\zeta_T|^\Xi - \alpha \cdot \zeta_T\big] \\ \leqslant -(\sigma_a + z_b)\eta_b \zeta_T - (\sigma_c + z_t)\eta_t \zeta_T - (\sigma_e + z_p)\eta_p \zeta_T \\ - \varpi \cdot |\zeta_T|^{\Xi + 1} - \alpha \cdot \zeta_T^2 \qquad (71)$$

where $\eta_b > 0$, $\eta_t > 0$, and $\eta_p > 0$ for finite-time bounded estimated disturbance error $|\xi_b| \leqslant \eta_b$, $|\xi_t| \leqslant \eta_t$, and $|\xi_p| \leqslant \eta_p$ respectively. In (71), the derivative of Lyapunov candidate is negative definite. From this, we can concluded that the total sliding surface is Lyapunov stable and it will not escape in finite time hence, the system dynamics will converge to zero in finite time.

Simulation results and discussions

To validate the proposed TORA based barge-type offshore floating wind turbine mathematical model and to compare the performance of DOBBSMC, DOBBISMC, DOBBNTSMC, and DOBBINTSMC algorithms for the stabilization of proposed OFWT, the simulations of close-loop control system are performed on MATLAB/SIMULINK. As a switching control, the chattering effect is the drawback of the signum function. According to the integral sliding mode control theory, for reducing this chattering effect from traditional backstepping sliding mode control and backstepping nonsingular terminal sliding mode control, we have taken integral terms into the sliding surfaces, which are based on the backstepping sates of OFWT. The proposed OFWT parameters for the
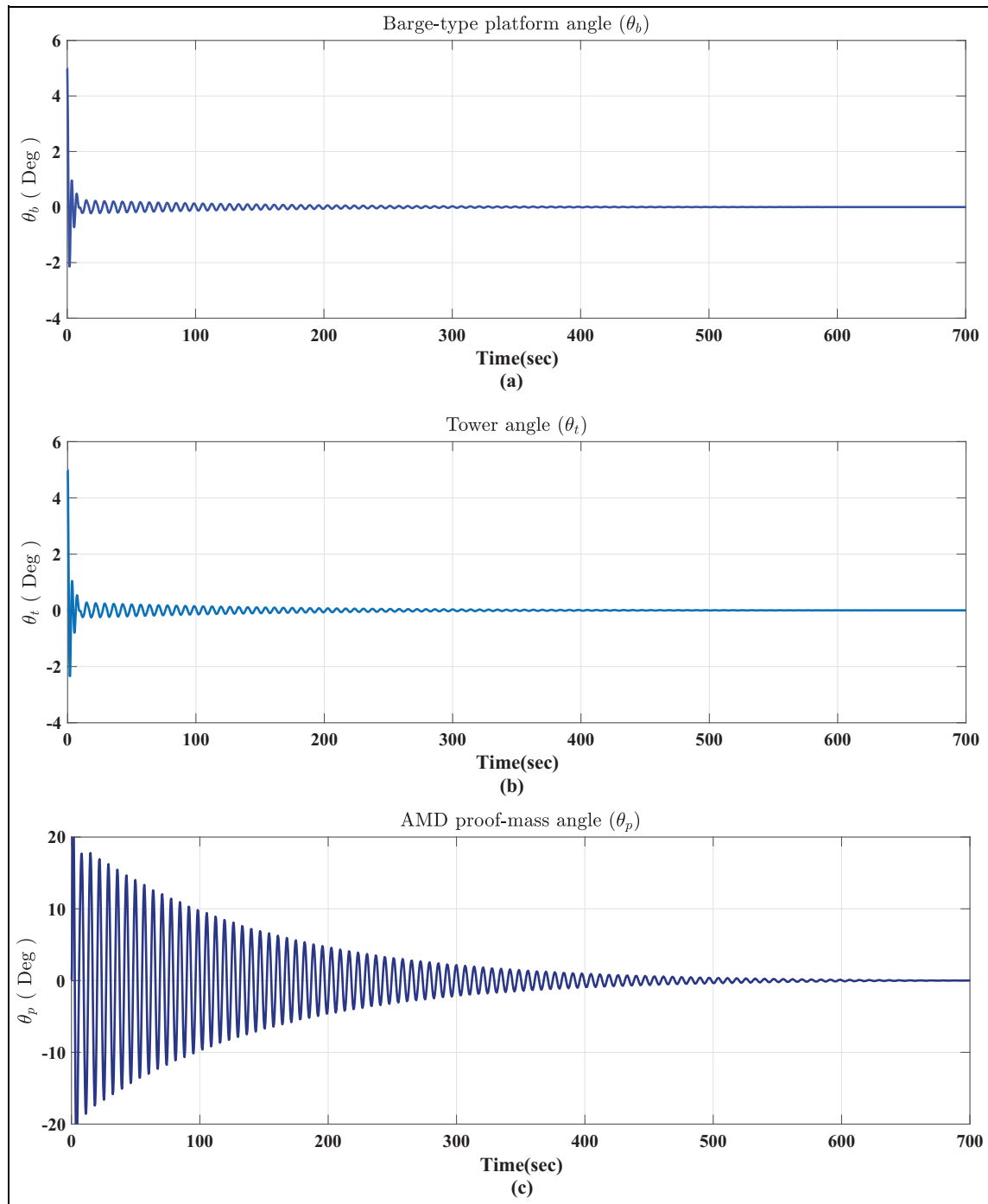
Figure 3. TORA based barge-type OFWT response without control input: (a) barge-type platform angle (θ_b), (b) tower angle (θ_t), and (c) AMD proof-mass angle (θ_p).

simulation study are described in Table 1. Since this article aims to verify the mathematical model and proposed model stabilization by applying different robust control laws, it is assumed that the angles are perturbed initially. Hence, the initial conditions are assumed as: $[x_a \ x_b \ x_c \ x_d \ x_e \ x_f]^T = [\pi/36 \ 0 \ \pi/36 \ 0 \ 0 \ 0]^T$.

From (a), (b), and (c) parts of Figure 3, it can be seen that by applying the above initial conditions and without control input, the barge-type platform, tower, and AMD proof-mass go back to their equilibrium

position in 400 s, 400 s, and 630 s respectively, after a certain amount of oscillations. Similarly, this model is valid for all the assumptions described in the modeling portion. To ensure the robustness property of all these four controllers along with finite time disturbance observer, a mismatched sinusoidal disturbance $\psi_i(t) = 5\sin(2\pi ft)$ is integrated into the system, where $i = b, t, p$, and $f = 15$ hertz. In Figure 4, to stabilize the proposed OFWT, a comparison analysis is performed between DOBBSMC, DOBBISMC, DOBBNTSMC,
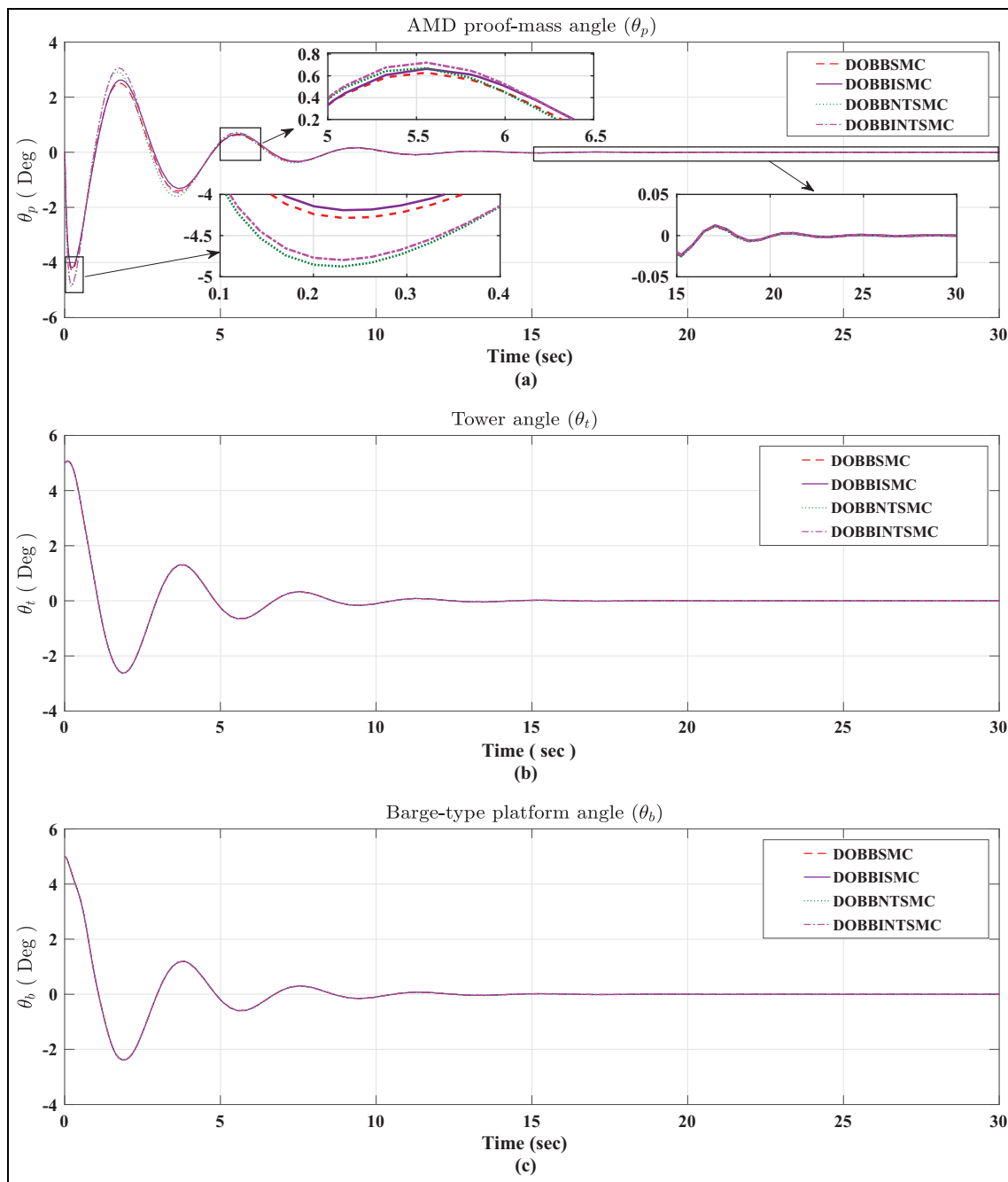
Figure 4. TORA based barge-type OFWT response with DO based control input (DOBBSMC, DOBBISMC, DOBBNTSMC, DOBBINTSMC): (a) AMD proof-mass angle (θ_p), (b) tower angle (θ_t), and (c) barge-type platform angle (θ_b).

and DOBBINTSMC. By using tuning parameters of Table 2, all these four control inputs are separately applied to AMD proof-mass actuator for controlling OFWT vibration. The transient response and steady-state response of AMD proof-mass state can be seen in Figure 4(a), which shows that all the four control laws have almost the same stabilization behavior with minor differences. It can be seen that the amplitude of the first peak of AMD proof-mass state for DOBBISMC and DOBBINTSMC is less as compare to DOBBSMC and DOBBNTSMC respectively. By using all these four control laws, the AMD proof-mass state goes toward

its equilibrium position and become stable after 25 s simultaneously. From Figure 4(b) and (c), we have observed that, through controlling the angular position of AMD proof-mass, we can able to control the tower and barge-type platform oscillation within 14.5 s for all four controlled input cases. All the four controlled input torques with a comparison to each other are shown in Figure 5, which are applied to the AMD proof-mass actuator for achieving desired control tasks. Here, we can see clearly that, unwanted chattering has occurred in all four control inputs with different amplitudes. In Figure 5(a), the performance of

Table 2. Tuning parameters of DO based control strategies.

Parameters	BSMC	BISMC	BNTSMC	BINTSMC
σ_a	3	3	3	3
σ_b	1	1	1	1
σ_c	5	5	5	5
σ_d	1	1	1	1
σ_e	2	2	2	2
σ_f	1	1	1	1
σ_g	-	2	-	2
σ_h	-	1	-	1
σ_i	-	4	-	4
Γ_1	1	1	1	1
Γ_2	3	3	3	3
Γ_3	10	10	10	10
$\varepsilon_1 = \varepsilon_2$	-	-	1	1
ε_3	-	-	100	100
$v_1 = v_2 = v_3$	-	-	7	7
$w_1 = w_2 = w_3$	-	-	5	5
ϖ	10	10	10	10
α	100	100	100	100
Ξ	-	-	0.5	0.5

DOBBISMC is better than DOBBSMC. In Figure 5(b), the performance of DOBBINTSMC is better than DOBBNTSMC. In Figure 5(c), the performance of DOBBISMC is better than DOBBINTSMC. Overall, DOBBISMC performance is better than the other three control inputs. Figure 6 shows the hierarchical total sliding mode surfaces of the proposed OFWT model for designing four control input laws. The disturbance estimation of three subsystems of the proposed OFWT model by using four disturbance observer-based control laws are shown in Figures 7 to 9. In the part (a) of Figures 7 to 9 the sinusoidal disturbance is estimated by finite time disturbance observer, which is almost same for all the three subsystems of OFWT model with following observer design constants, that is, $\Delta_0 = \Delta_1 = \Delta_2 = \Delta_3 = \Delta_4 = \Delta_5 = \Delta_6 = \Delta_7 = \Delta_8 = 200$, where $\hbar = 10$. The error of estimated disturbance to the sinusoidal disturbance for four DO based control laws are shown in (b) part of Figures 7 to 9. The estimation error in the form of root mean square (RMS)
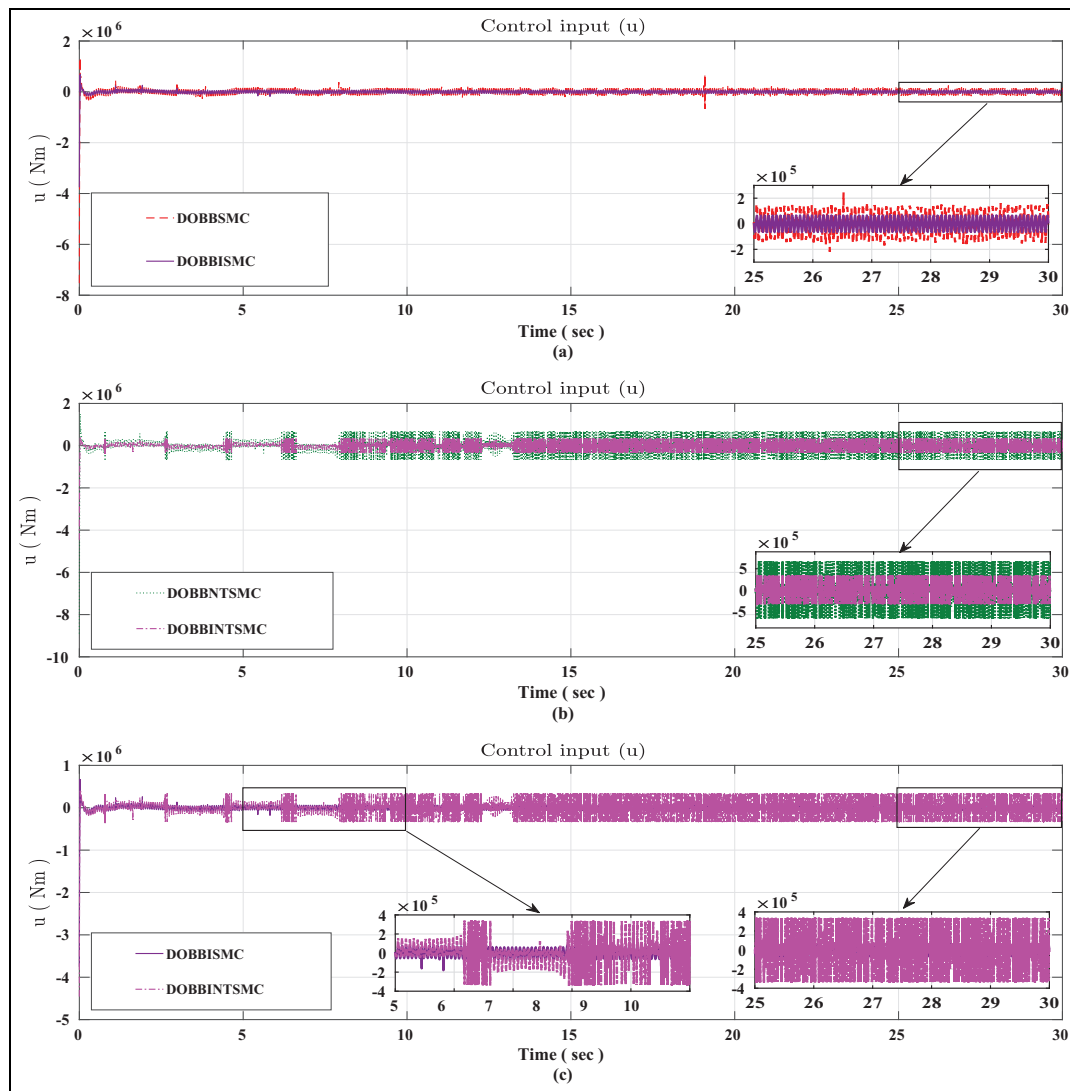
Figure 5. Comparison of disturbance observer based control input: (a) DOBBSMC vs DOBBISMC, (b) DOBBNTSMC vs DOBBINTSMC, and (c) DOBBISMC vs DOBBINTSMC.
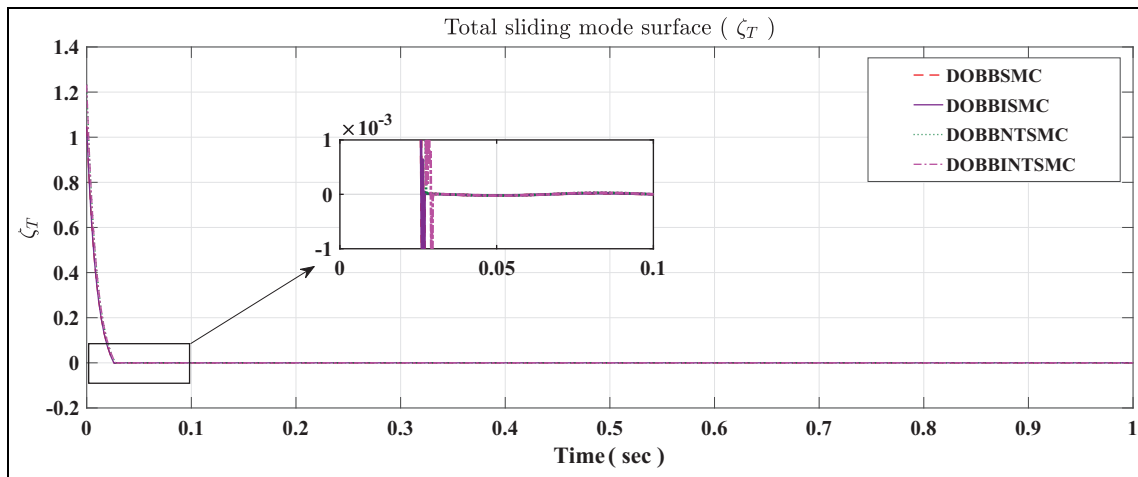
Figure 6. Total sliding mode surface (ζ_T) for designing DOBB-SMC, DOBBISMC, DOBBNTSMC, and DOBBINTSMC laws.
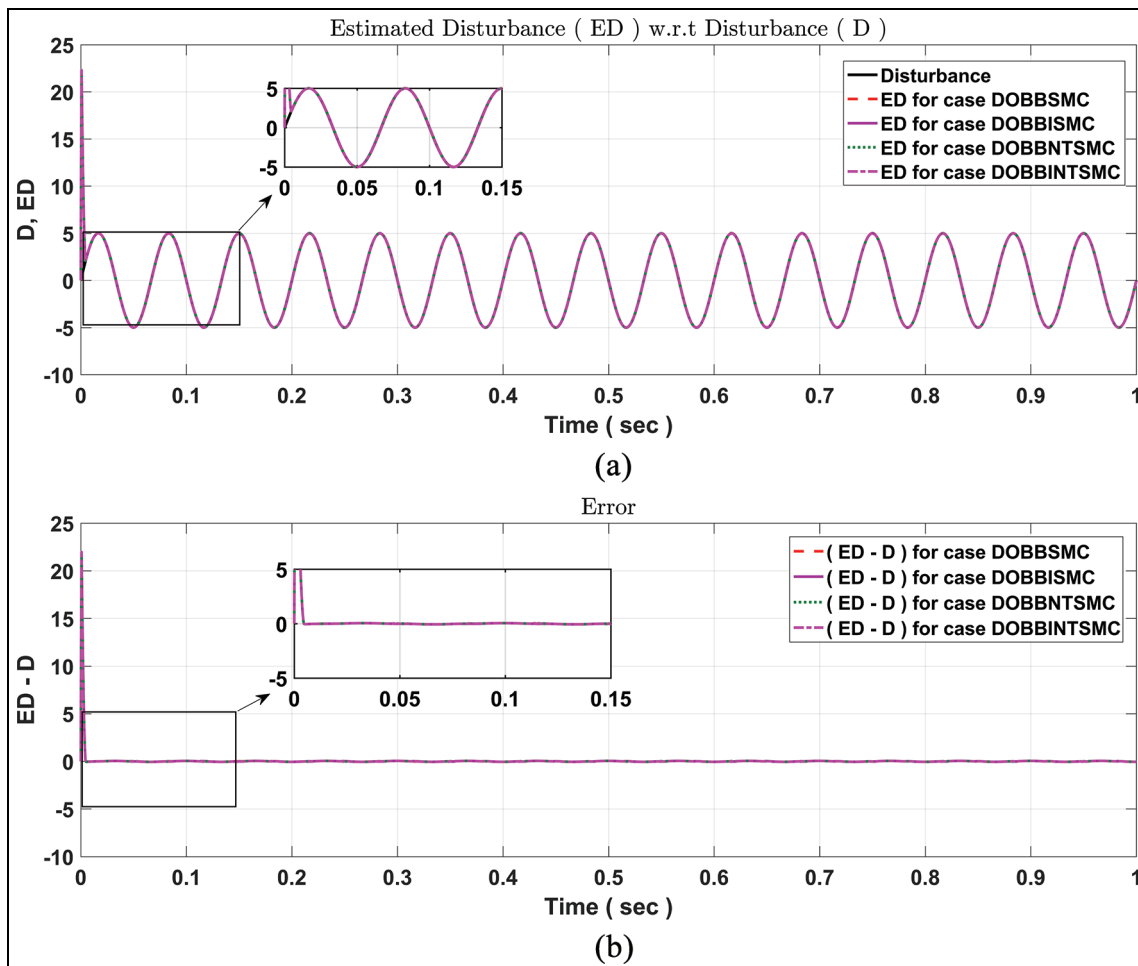

Figure 7. Disturbance estimation of the subsystem (platform) by using different control inputs: (a) estimated disturbance (ED) with respect to disturbance (D) and (b) error of estimated disturbance with respect to disturbance.

of all the subsystems for each control input is mention in Table 3. It is evident from all these simulation results that hierarchical DOBBSMC, DOBBISMC, DOBBNTSMC, and DOBBINTSMC algorithms dealt very efficiently with such a perturbed system. Moreover, overall the DOBBISMC shows relatively better performance in terms of transient and steady-state response.
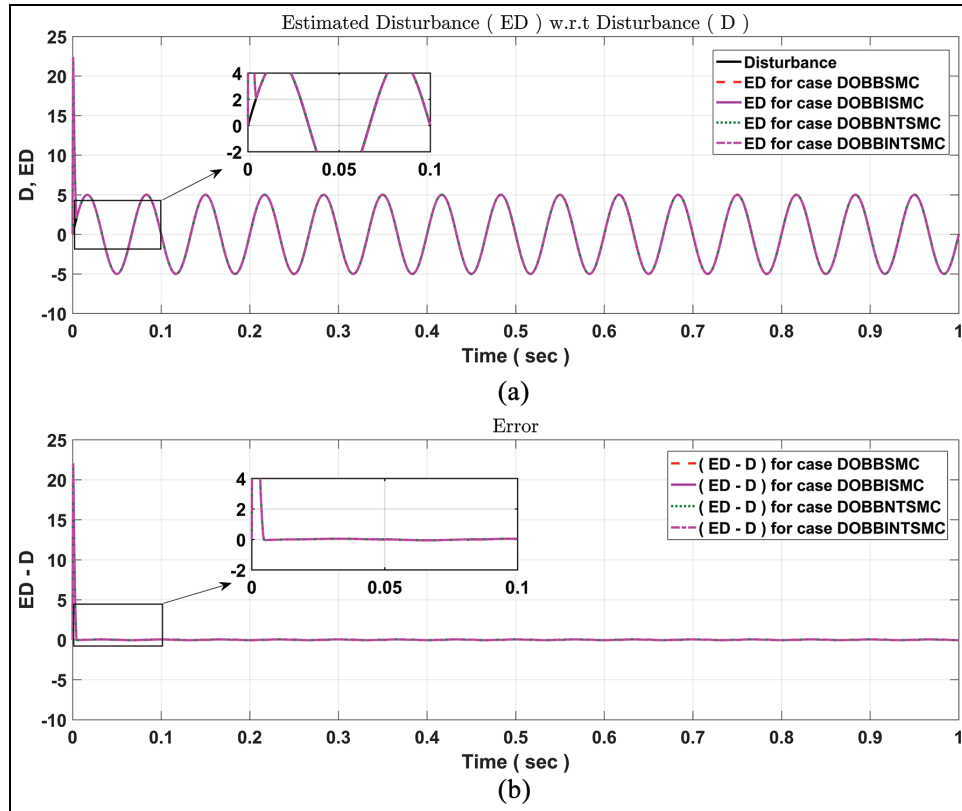
Figure 8. Disturbance estimation of the subsystem (tower) by using different control inputs: (a) estimated disturbance (ED) with respect to disturbance (D) and (b) error of estimated disturbance with respect to disturbance.
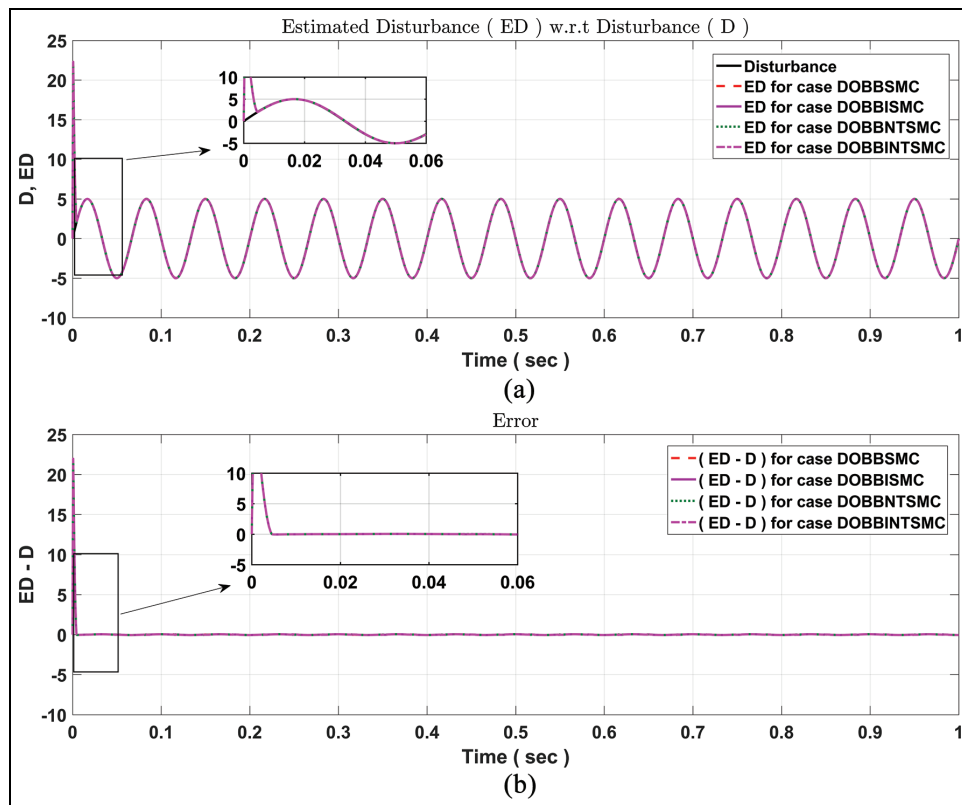

Figure 9. Disturbance estimation of the subsystem (AMD proof-mass) by using different control inputs: (a) estimated disturbance (ED) with respect to disturbance (D) and (b) error of estimated disturbance with respect to disturbance.

Table 3. Estimation error (RMS) of all the subsystems for each control input.

Control input	Subsystem (Platform)	Subsystem (Tower)	Subsystem (AMD Proof-mass)
BSMC	0.69791439	0.76453999	0.78169851
BISMC	0.69791149	0.76453671	0.78169325
BNTSMC	0.69791724	0.76453454	0.78169714
BINTSMC	0.69791654	0.76453352	0.78169633

Conclusion

In this paper, a new active control strategy (TORA) is adopted in the barge-type offshore floating wind turbine for the vibration mitigation purpose. The mathematical model of the proposed TORA based barge-type OFWT is established by using Lagrange equations. Before controlling the proposed OFWT, the system equilibrium points are determined and then four robust control algorithms (DOBBSMC, DOBBISMC, DOBBNTSMC, DOBBINTSMC) are designed for the proposed model stabilization in the presence of mismatched disturbances. The verification of the mathematical model and comparative analysis of robust control techniques are performed by using the standard tool MATLAB/SIMULINK. For the comparison purposes, through using the same control tuning parameters for all the four control strategies, we have observed from simulation results that all four robust control laws stabilized the proposed model simultaneously and overall DOBBISMC shows better performance as compared to the other three control strategies.

ORCID iD

Bingtuan Gao (iD) https://orcid.org/0000-0001-6933-0743

References

1. Leung DYC and Yang Y. Wind energy development and its environmental impact: a review. *Renew Sust Energ Rev* 2012; 16(1): 1031–1039.
2. Snyder B and Kaiser MJ. Ecological and economic cost-benefit analysis of offshore wind energy. *Renew Energ* 2009; 34(6): 1567–1578.
3. Kaldellis JK and Kapsali M. Shifting towards offshore wind energy–recent activity and future development. *Energy Policy* 2013; 53: 136–148.
4. Pérez–Collazo C, Greaves D and Iglesias G. A review of combined wave and offshore wind energy. *Renew Sust Energ Rev* 2015; 42: 141–153.
5. Li X and Gao H. Mitigation for a floating wind turbine via generalized H∞ structural control. *IEEE Trans Ind Electron* 2015; 63(1): 332–342.
6. Lackner MA and Rotea MA. Structural control of floating wind turbines. *Mechatronics* 2011; 21(4): 704–719.
7. Butterfield S, Musial W, Jonkman J, et al. Engineering challenges for floating offshore wind turbines. In: *2005 Copenhagen offshore wind conference*, Copenhagen, Denmark, September 2007, No: NREL/CP-500-38776. Golden, CO: National Renew Energy Lab (NREL).
8. Spencer JBF and Nagarajaiah S. State of the art of structural control. *J Struct Eng* 2003; 129(7): 845–856.
9. Singh MP, Matheu EE and Suarez LE. Active and semi-active control of structures under seismic excitation. *Earthquake Eng Struct Dynam* 1997; 26(2): 193–213.
10. Soong TT and Spencer JBF. Supplemental energy dissipation: state-of-the-art and state-of-the practice. *Eng Struct* 2002; 24(3): 243–259.
11. Ni YQ, Ying ZG, Wang JY, et al. Stochastic optimal control of wind-excited tall buildings using semi-active MR-TLCDs. *Eng Mech* 2004; 19(3): 269–277.
12. Hirayama T and Ma N. Dynamic response of a very large floating structure with active pneumatic control. In: *The seventh international offshore and polar engineering conference*, Honolulu, Hawaii, 25–30 May 1997. International Society of Offshore and Polar Engineering.
13. Dyke SJ, Spencer JBF, Quast P, et al. Implementation of an active mass driver using acceleration feedback control. *Comput-Aided Civ Inf* 1996; 11(5): 305–323.
14. Murtagh PJ, Ghosh A, Basu B, et al. Passive control of wind turbine vibrations including blade/tower interaction and rotationally sampled turbulence. *Wind Energy* 2008; 11(4): 305–317.
15. Stewart GM. *Load reduction of floating wind turbines using tuned mass dampers*. MSc Thesis, University of Massachusetts, Amherst, MA, 2012.
16. He EM, Hu YQ and Zhang Y. Optimization design of tuned mass damper for vibration suppression of a barge-type offshore floating wind turbine. *Proc IMechE, Part M: J Engineering for the Maritime Environment* 2017; 231(1): 302–315.
17. Yang J, He EM and Hu YQ. Dynamic modeling and vibration suppression for an offshore wind turbine with a tuned mass damper in floating platform. *Appl Ocean Res* 2019; 83: 21–29.
18. Huang C, Arrigan J, Nagarajaiah S, et al. Semi-active algorithm for edgewise vibration control in floating wind turbine blades. In: *The 12th biennial international conference on engineering, construction, and operations in challenging environments*, Honolulu, Hawaii, 14–17 March 2010, pp.2097–2110.
19. Arrigan J, Pakrashi V, Basu B, et al. Control of flapwise vibrations in wind turbine blades using semi-active tuned mass dampers. *Struct Control Health Monit* 2011; 18(8): 840–851.
20. Dinh VN and Basu B. Passive control of floating offshore wind turbine nacelle and spar vibrations by multiple tuned mass dampers. *Struct Control Health* 2015; 22(1): 152–176.
21. Sun C. Semi-active control of monopile offshore wind turbines under multi-hazards. *Mech Syst Signal Process* 2018; 99: 285–305.

22. Park S, Lackner MA, Cross-Whiter J, et al. An investigation of passive and semi-active tuned mass dampers for a tension leg platform floating offshore wind turbine in ULS conditions. In: *ASME 2016, 35th international conference on ocean, offshore mechanics and arctic engineering*, Busan, South Korea, 19–24 June 2016. The American Society of Mechanical Engineers Digital Collection.

23. Si Y and Karimi HR. Gain scheduling H_2/H_∞ structural control of a floating wind turbine. *Proc IFAC World Congress* 2014; 47(3): 6788–6793.

24. Hu Y and He E. Active structural control of a floating wind turbine with a stroke-limited hybrid mass damper. *J Sound Vib* 2017; 410: 447–472.

25. Fitzgerald B, Sarkar S and Staino A. Improved reliability of wind turbine towers with active tuned mass dampers (ATMDs). *J Sound Vib* 2018; 419: 103–122.

26. He B, Wang S and Liu Y. Underactuated robotics: a review. *Int J Adv Rob Sys* 2019; 16(4): 1–29.

27. Wan CJ, Bernstein DS and Coppola VT. Global stabilization of the oscillating eccentric rotor. *Nonlinear Dyn* 1996; 10(1): 49–62.

28. Yu Z, Yuan-bo G and Xiao-hua Z. Stability control of TORA with environmental disturbance. In: *The 27th Chinese Control and Decision Conference (CCDC)*, Qingdao, China, 23–25 May 2015, pp.6107–6110. New York: IEEE.

29. Bao Y, Jia L, Xie J, et al. On hierarchical sliding mode control of underactuated TORA system. In: *Proceedings of the 10th World Congress on Intelligent Control and Automation*, Beijing, China, 6–8 July 2012, pp.1785–1789. New York: IEEE.

30. Bayramoglu H and Komurcugil H. Nonsingular decoupled terminal sliding-mode control for a class of fourth-order nonlinear systems. *Commun Nonlinear Sci Numer Simul* 2013; 18(9): 2527–2539.

31. Rudra S, Barai RK and Maitra M. *Block backstepping design of nonlinear state feedback control law for underactuated mechanical systems*. Singapore: Springer, 2017.

32. Liu C, Gao B, Zhao J, et al. Orbitally stabilizing control for the underactuated translational oscillator with rotational actuator system: design and experimentation. *Proc IMechE, Part I: J Systems and Control Engineering* 2019; 233(5): 491–500.

33. Ullah S, Khan Q, Mehmood A, et al. Integral backstepping integral sliding mode control of underactuated nonlinear electromechanical systems. *Control Eng Appl Inf* 2019; 21(3): 42–50.

34. Yang F, Song QW, Wang L, et al. Wind and wave disturbances compensation to floating offshore wind turbine using improved individual pitch control based on fuzzy control strategy. *Abstr Appl Anal*. Epub ahead of print 30 March 2014. DOI: 10.1155/2014/968384.

35. Raach S, Schlipf D, Sandner F, et al. Nonlinear model predictive control of floating wind turbines with individual pitch control. In: *American control conference*, Portland, OR, 4–6 June 2014, pp.4434–4439. New York: IEEE.

36. Zhang C, Tahoumi E, Gutierrez S, et al. Adaptive robust control of floating offshore wind turbine based on sliding mode. In: *58th conference on decision and control (CDC)*, Nice, France, 11–13 December 2019, pp.6936–6941. New York: IEEE.

37. Shtessel YB, Shkolnikov IA and Levant A. Smooth second-order sliding modes: missile guidance application. *Automatica* 2007; 43(8): 1470–1476.

38. Li S, Yang J, Chen WH, et al. *Disturbance observer-based control: methods and applications*. Boca Raton, FL: CRC press, 2014.